Chapter 4

Mechanical Performance of Simple Supported Concrete Beam-Cable Composite Element with External Prestress

Teng Wang, Yanmei Ding, Wangchun Zhang and Yu Song

Additional information is available at the end of the chapter

http://dx.doi.org/10.5772/intechopen.76517

Abstract

A new reinforcement technology of external prestress based on stretch tilted belly poles has been presented. Taking simply supported beam, which is reinforced by three titled belly poles, as a research object to establish a model of reinforced simply supported beam. Relationship expressions about deflection and internal force increment of external cable or about load and deflection have been deduced. Finite element model is established by ABAQUS. The influence of structure performance of reinforced simply supported beam with cable section, cable sag and initial internal force value was investigated. Three tests are carried out to testify the results of theoretical analysis and numerical simulation. The results show that the redistributions of internal force and sectional stress have occurred, and the stiffness, crack load, ultimate load, and structure ductility are all improved with the increase of three design parameters. For example, the crack load, ultimate load, and structure ductility have increased, respectively, by 24%~40%, 15%~42%, and 14%~40%. High initial internal force, small section, and big cable sag should be avoided, because the probability of brittle failure of structure will increase. The analytical result shows that the reliability of internal increment expression of external cable and carrying capacity expression can be used in the engineering practice.

Keywords: concrete structure, simply supported beam, external prestress, tilted belly poles, test

1. Introduction

External prestressing is a technique originally developed for reinforcing bridge structures and now has applications in architectural structures [1]. It has gone through three stages of development. In the early stage, external tendons were installed with curvature at the bottom and sides of a beam and held by deviators. Prestressing forces were applied by transverse tensioning. In the second stage, external tendons were installed with curvature only at the vertical sides of a beam, and prestressing forces were applied by a tensioning jack. Multiple weaknesses have been identified in this tensioning technique during practical applications. First, prestressing forces had to be applied to an independent working surface, but the working surface was usually obstructed by columns. Second, the friction between a deviator and an external tendon could weaken the effects of prestressing forces. To avoid the aforementioned problem with working surface, external tendons were usually continuously and axially installed along the full length of a beam. However, this would complicate the stress states of the columns and beam-column joints and thereby undermine the structure's seismic performance [2]. To overcome these disadvantages, retractable web members were introduced to apply prestressing forces in the later stage. Web members can be installed vertically or diagonally, and DWMs are an improvement on vertical web members (patent number: ZL 03134360.0). In DWM prestressing, external tendons are anchored to the upper parts of both beam sides, and retractable DWMs are used to stretch the tendons, which then transfer the prestressing forces to the beam. Compared to the two earlier external prestressing techniques, DWM prestressing has two main advantages: (1) The way in which the prestressing force is applied allows for easier and safer construction and enhances the effects of prestressing forces; (2) As external tendons are not continuously installed along the full beam length and do not span any column, the installation process will neither cause mechanical disturbance to the floor, columns, and other vertical elements nor occupy the space required to reinforce vertical elements; (3) external tendons running through beam ends can increase the shear strength of beam ends [3, 4].

At present, stress increments in external tendons can be calculated mainly by the reduction factor method, regression analysis of section reinforcement ratio, deformation analysis, and so on. However, there is a lack of unified standard and the standard parameter values for an external tendon in the stiffness of a beam is infinitely great an ultimate state differ between standards from different countries [5–8]. Based on the assumption of infinite beam stiffness, a study [9] examined the force distribution in an external tendon that was subjected to a uniformly distributed load applied by DWM, with the increase in tendon length being used as the parameter. The relationship between tendon extension and load was derived. When DWM external prestressing is applied to a simply supported beam (SSB), the beam does not have infinite stiffness and tends to deform under the prestressing force [10, 11]. The load on tendons applied by web members was not uniformly distributed. Therefore, the mechanical behavior of a beam reinforced by this technique remains unknown. For this reason, the present study investigated the behavior of a SSB reinforced by external prestressing with three DWMs using a combination of theoretical derivation, numerical analysis, and experimental verification. Three variables, including initial tendon force, tendon cross-sectional area, and initial tendon sag, were considered and the influences of beam-end rotation and beam

http://dx.doi.org/10.5772/intechopen.76517

deflection on tendon force were analyzed. Then the pattern of variation in the RC beam's structural performance was obtained. The findings of the study are expected to provide a design basis for practical application of this technique and theoretical support for research on the mechanical behavior of a fixed-end beam after reinforcement.

2. Theoretical analysis

2.1. Increment in tendon stress

2.1.1. Fundamental assumptions

The theoretical analysis was based on the following fundamental assumptions:

1. An external tendon is an ideally flexible material subjected only to tension, and it deforms only elastically throughout its deformation process;
2. The web members have infinite stiffness and do not stretch or shrink during beam deformation. They are always perpendicular to the tangents at the connections between web members and tendons. The effect of dead load of web members on tendons is ignored;
3. The slip between external tendons and web members during beam deformation is negligible and so is the friction between tendons and beam-end anchorage and between web members and beam-bottom anchorage. The shear deformation of the beam, together with its secondary effect, has only negligibly small effects on RC beam.
4. The load applied to an external tendon by the three DWMs can be treated as a uniformly distributed load.

2.1.2. Computing model of tendon

Figure 1 shows the curves describing deformation of an external tendon in a SSB reinforced by DWM prestressing. The dotted line L_1 shown in the figure is the elliptic curve describing the deformation of a tendon under a uniformly distributed load provided in [9]. The solid line, L_2, is a broken line for a tendon stabilized by three web members; it is a polygon incised in L_1.

2.1.3. Solving for external tendon force

According to Song Yu [9], the shape function for a tendon under a uniformly distributed load has the following form:

$$\frac{\left(y-\frac{l^2-8f^2}{16f}\right)^2}{\left(\frac{l^2+8f^2}{16f}\right)^2}+\frac{\left(x-\frac{l}{2}\right)^2}{2\left(\frac{l^2+8f^2}{16f}\right)^2}=1 \tag{1}$$

where l and f are the tendon span and sag, respectively, after application of the initial prestressing force.

Let $m = \frac{l^2 + 8f^2}{16f}$ and compute the derivative of the shape function with respect to x. Then performing integration on the arc-length formula will yield the expression for initial tendon length, s_o:

$$s_0 = \frac{3l}{4} + \frac{\sqrt{2}\,m}{4} + \ln\frac{2\sqrt{2}\,m + l}{2\sqrt{2}\,m - l} \tag{2}$$

When the SSB undergoes a beam-end rotation of θ under the action of an external load, the resulting span and sag of each tendon can be expressed as follows:

$$L' = l - 2 \cdot e \cdot \sin\theta \tag{3}$$

$$f = f + y \tag{4}$$

where e is the initial eccentricity of external tendon and y is the deflection of the beam under the action of an external load.

Change in tendon length is associated with tendon span and sag. After the SSB deforms, both the tendon span and sag will change. Substituting Eqs. (3) and (4) into Eq. (2) will give the tendon length for a given beam deflection.

$$s = \frac{3L'}{4} + \frac{\sqrt{2}\,m'}{4} + \ln\frac{2\sqrt{2}\,m' + L'}{2\sqrt{2}\,m' - L'} \tag{5}$$

where $m' = \frac{L'^2 + 8f'^2}{16f}$.

Since the behavior of external tendons is always elastic, according to the Hooke's law,

$$\Delta S = S - S_0 \tag{6}$$

$$\Delta S = \frac{\Delta F}{EA_s}.S_0 \tag{7}$$

$$p_s = P_0 + \Delta F \tag{8}$$

where Δs is tendon extension, ΔF is the increment in tendon force, E is tendon's elastic modulus, A_s is tendon cross-sectional area, s_0 is initial tendon length, and p_S is the tendon force for a given beam deflection.

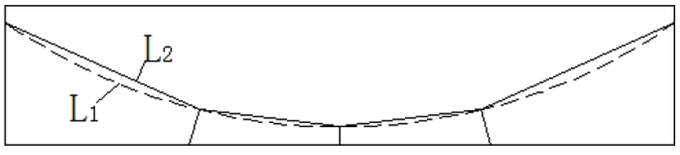

Figure 1. The external cable diagram of deformation.

http://dx.doi.org/10.5772/intechopen.76517

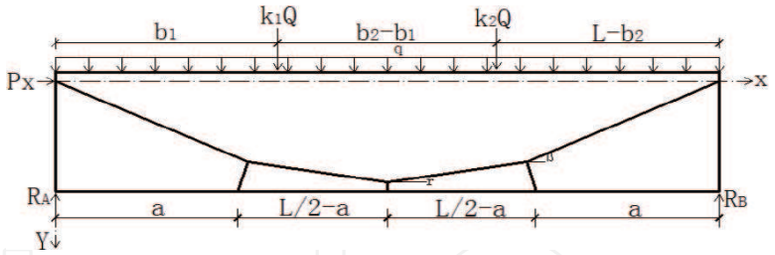

Figure 2. Analysis diagram of beam-cable element.

2.2. Calculation of bearing capacity of a RC beam during normal service

2.2.1. Computing model

After a SSB is reinforced by DWM external prestressing, the main forces acting on it include constant and live loads (e.g., concentrated force, $ki{\cdot}Q$, and uniformly distributed load, q), prestressing force on the beam exerted by tendons, p_s, reaction forces from the supports, and concentrated forces exerted on the beam by web members. This analysis focused on two randomly selected concentrated forces. The force analysis and the coordinate system used are presented in **Figure 2**.

2.2.2. Load-deformation relationship

Let EI denote the flexural rigidity of a beam within its elastic range and e be the initial eccentricity of tendon. The force applied by a DWM can be decomposed into two components. This analysis did not consider the effect of the horizontal component on the beam's mechanical behavior in order to simplify the calculation. The analytical results proved reliable. Normally, the use of n web members will divide a beam into four segments. Thus three web members divide the beam into four segments. Computing the moment at an arbitrary cross-section of the beam gives

$$EI \cdot y'' = \frac{qx(l-x)}{2} + k_i Q \cdot \sum_{i=1}^{n} f(x) - p_s \cdot m(x) - p_s \cdot (e+y) \cdot \cos\gamma \tag{9}$$

where

$$f(x) = \begin{cases} x(l-b_i)/l & (0 \le x \le b_i) \\ b_i(l-x)/l & (b_i \le x \le l) \end{cases} \tag{10}$$

$$m(x) = \begin{cases} x\sin\gamma & (0 \le x \le a) \\ -(x-a)(\sin\gamma - \sin\beta) + x\sin\gamma & (a \le x \le a + l' \cdot \sin\varphi) \\ -(x-a)(\sin\gamma - \sin\beta) + x\sin\beta & (a + l' \cdot \sin\varphi \le x \le l/2) \\ -(l-x-a)(\sin\gamma - \sin\beta) + (l-x)\sin\beta & (l/2 \le x \le l - a - l' \cdot \sin\varphi) \\ -(l-x-a)(\sin\gamma - \sin\beta) + (l-x)\sin\gamma & (l - a - l' \cdot \sin\varphi \le x \le l - a) \\ (l-x)\sin\gamma & (l - a - l' \cdot \sin\varphi \le x \le l) \end{cases} \tag{11}$$

where l' is the length of a DWM, Φ is the angle between the DWM and the y-axis, ki is a load factor, bi is the distance from the concentrated load to the support, r is the angle between the midspan web member and the horizontal plane at its intersection with the tendon, and β is the angle between the DWM and the horizontal plane at its intersection with the tendon.

By taking the partial derivative of formula (9), we obtain

$$y(x) = e\left[\frac{\cos\omega(x-\frac{l}{2})}{\cos(\frac{\omega l}{2})}-1\right]+\frac{q}{p_s\cdot\cos\gamma}\cdot\left\{\frac{x}{2}(l-x)-\frac{1}{\omega^2}\left[\frac{\cos\omega(x-\frac{l}{2})}{\cos(\frac{\omega l}{2})}-1\right]\right\}$$
$$+\frac{Q}{p_s\cdot\cos\gamma}\sum_{i=1}^{2}k_i\cdot f(x)-\frac{1}{\cos\gamma}\cdot m(x) \tag{12}$$

where

$$\omega = \sqrt{\frac{p_s}{EI}\cos\gamma} \tag{13}$$

Eq. (12) describes the relationship between external load and RC beam deflection, which can be used as a theoretical basis for design of SSB reinforced by external prestressing with three web members.

3. Finite element analysis

3.1. Constitutive relations

A model of an RC beam reinforced by external prestressing was constructed by separate modeling using ABAQUS, a software suite for finite element analysis. The concrete was modeled using C3D8R, a linear reduced integration element with eight nodes. The rebars, web members, and external tendons were constructed of T3D2, a three-dimensional, two-node linear truss element. The slip between rebars and concrete was neglected. The constraints between the concrete and reinforcement cage were applied via the Embedded Region command. The constraint relationships between external tendon and concrete beam and between web members and concrete beam were achieved via the Kinematic coupling command. External prestressing force was applied by decreasing the temperature and solved by an implicit solver

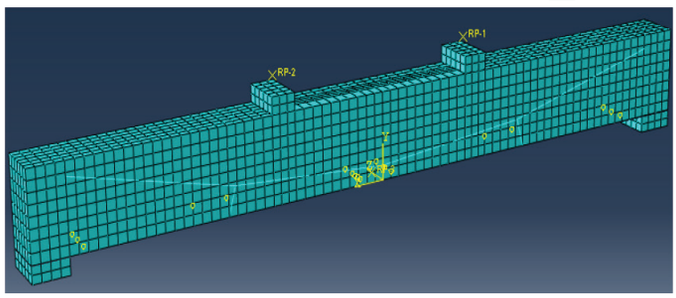

Figure 3. Finite element model. (a) Concrete, (b) steel reinforcement, (c) web member.

http://dx.doi.org/10.5772/intechopen.76517

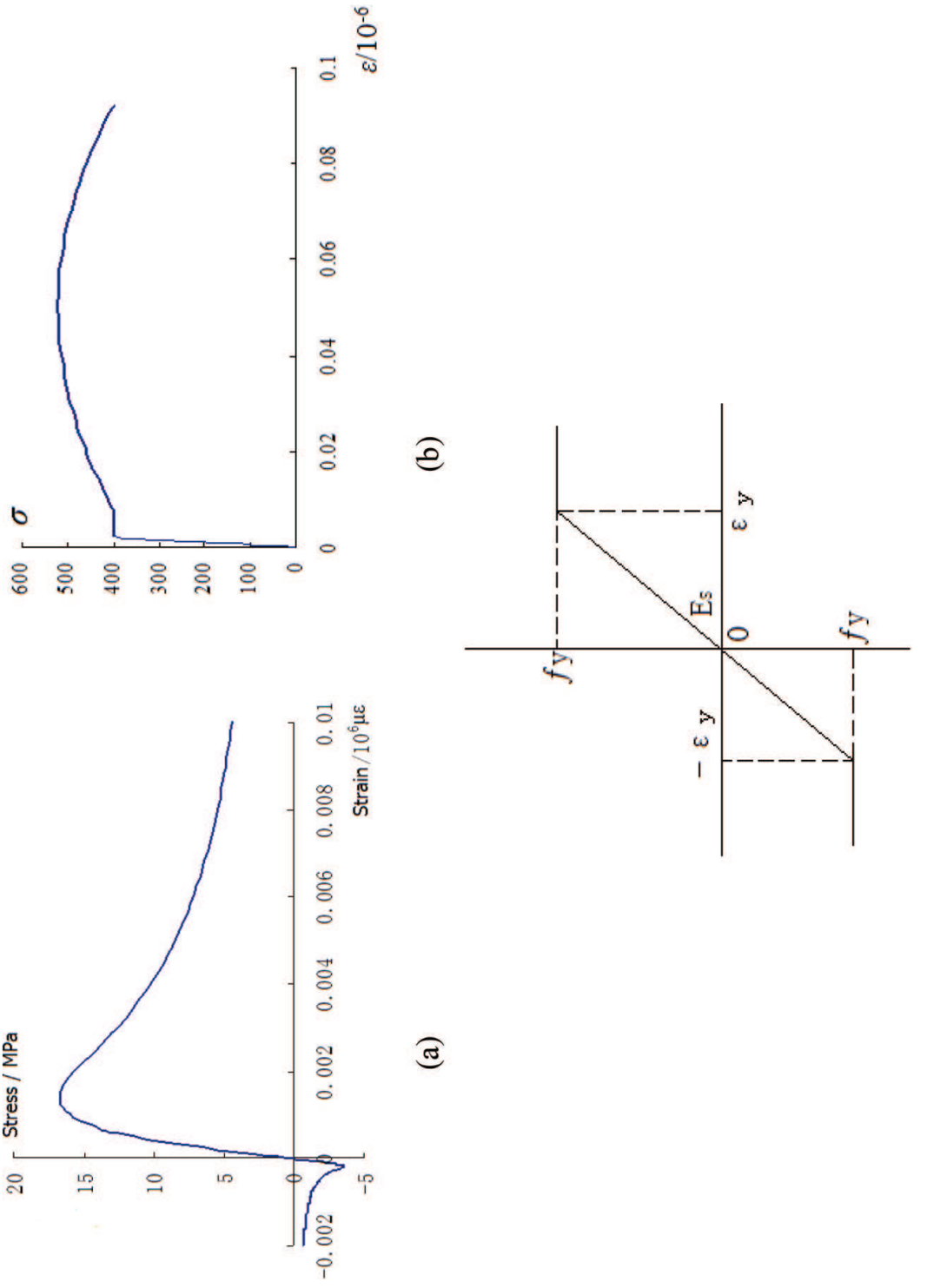

Figure 4. The material stress–strain curve.

(**Figure 3**). The concrete was modeled with the plastic damage constitutive model provided in ABAQUS, the rebars were modeled with the improved rebar model developed by Esmaeily-xiao, and the web members were simulated using an ideally elastic-plastic model. The constitutive relations for the model materials are presented in **Figure 4**.

3.2. Parameter design

The beam had dimensions of 3000 × 300 × 180 mm. It was constructed of C25 concrete, three Φ14 rebars in the concrete under tension, two vertical Φ14 rebars in the concrete under compression, Φ6 stirrups @100, and Φ14 web members (threaded). Design levels of the tendon parameters considered are as follows: initial tendon force, Level 3; tendon cross-sectional area, Level 3 (**Table 1**); and tendon sag, Level 4. Design values of other parameters are given in the first five lines of **Table 2**. FJGL denotes a control specimen, which was unreinforced. *denotes a specimen to be tested in the experimental verification.

3.3. Numerical results

3.3.1. Common features

The load-deflection curve for a RC beam generally splits into four portions. The characteristics of the four portions and the corresponding stages of the beam's behavior are summarized below:

1. Elastic deformation. In this stage, the concrete at the beam bottom slightly deflected without fracturing and the corresponding portion of the load-deflection curve is nearly linear;
2. Yielding. As the load increased, the bottom concrete showed increased deflection as a result of cracking. The rebars in the tensioned region reached the yield point earlier than the external tendons. The corresponding portion of the load-deflection curve contained a noticeable turning point;
3. Hardening. The neutral axis of a cross-section shifted downward and the external tendons were fully engaged in the work;
4. Failure. As the load continued increasing, the external prestressing tendon or the concrete under compression would fail after the tendon stress exceeded its ultimate strength or the compressive stress in the concrete exceeded its compressive strength. Their failure modes are different: the tendons failed via brittle fracture, while the concrete failed by ductile fracture.

No.	Cable diameter (mm)	Sectional area of cable (mm^2)	Breaking force (kN)
1	Φ9	48	75
2	Φ12	86	133
3	Φ15	134	208

Table 1. Design parameters of pre-stressed cables.

http://dx.doi.org/10.5772/intechopen.76517

Beam number	Cable sectional area (mm^2)	Sag of cable (mm)	Initial		Comparison of bearing capacity of simulated specimens			
			Cable internal force (kN)	Percent (%)	L/300 hour (kN)	Percentage increase (%)	L/200 hour (kN)	Percentage increase (%)
FJGL	/	/	/	/	90	/	105	/
JGL-1-1*	48	200	20	27	97	8	116	10
JGL-1-2	48	200	30	40	110	22	121	15
JGL-1-3	48	200	40	53	116	29	128	22
JGL-1-4	48	200	60	80	125	39	143	36
JGL-2-1	86	200	20	15	108	20	120	14
JGL-2-2	86	200	40	30	121	34	135	29
JGL-2-3	86	200	60	45	130	44	150	43
JGL-3-1	134	200	20	10	110	22	122	16
JGL-3-2	134	200	40	20	126	40	138	31
JGL-3-3	134	200	60	29	134	48	153	46
JGL-4-1	48	250	20	27	100	11	120	14
JGL-4-2	48	250	40	53	118	31	138	31
JGL-4-3	48	250	60	80	136	51	152	45
JGL-5-1	134	250	20	10	114	27	124	18
JGL-5-2	134	250	30	15	125	39	130	24
JGL-5-3	134	250	40	20	135	50	142	35
JGL-5-4	134	250	60	29	146	62	157	50
JGL-6-1	48	300	20	27	108	20	127	21
JGL-6-2	48	300	40	53	125	39	150	43
JGL-6-3	48	300	60	80	143	59	166	58
JGL-7-1	134	300	20	10	120	33	144	37
JGL-7-2	134	300	40	20	148	65	165	58
JGL-7-3	134	300	60	29	164	82	190	81
JGL-8-1	48	400	20	27	113	26	135	29
JGL-8-2	48	400	40	53	130	44	165	57
JGL-8-3	48	400	60	80	155	72	185	76
JGL-9-1	134	400	20	10	153	70	200	90
JGL-9-2	134	400	40	20	190	111	230	119
JGL-9-3	134	400	60	29	237	163	260	147

*Indicates the test specimen to be tested.

Table 2. Simply supported beam's design parameters and change of bearing capacity.

3.3.2. Relationship between beam deflection and increment in tendon force

1. The greater the initial tendon force, the smaller the maximum tendon deflection (or a tendon's energy dissipation capacity). **Figure 5a** shows the tendon force-deflection curves of a tendon with a cross-sectional area of 48 mm^2 and sag of 200 mm for different initial tendon forces (20, 40, and 60 kN). It is clear that the maximum tendon deflection at the fracture point gradually decreased. This implies that it is unreasonable to optimize reinforcement design simply by increasing the initial tendon force.
2. As the tendon cross-sectional area increased, the rate of growth in tendon force increased, and thus the contribution by the tendon became more significant. Conversely, a smaller tendon cross-sectional area is associated with a slower rate of increase in tendon force. **Figure 5b** illustrates the tendon force-deflection curves for different tendon cross-sectional areas (48, 86, and 134 mm^2) when the tendon sag was 200 mm and initial tendon force was 20 kN. This figure demonstrates that a larger tendon cross-sectional area is better in reinforcement design.

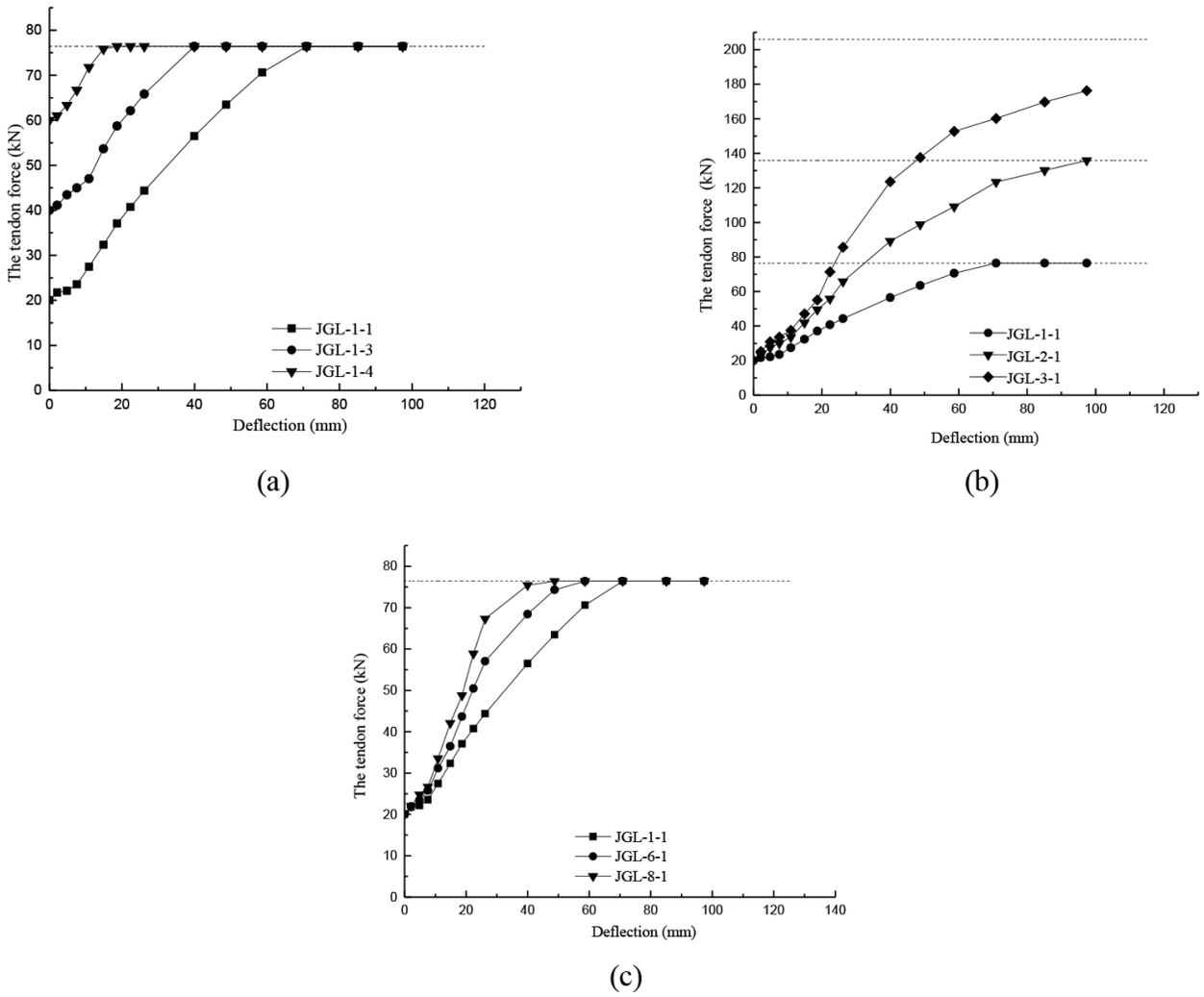

Figure 5. Cable internal force deflection curve. (a) The initial tendon force, (b) sectional area of cable, and (c) sag of cable. *The horizontal dotted line represents the tensile force at which the external prestressing tendon begins to fracture.

http://dx.doi.org/10.5772/intechopen.76517

3. The rate of tendon force growth increased with increasing tendon sag. **Figure 5c** shows the tendon force deflection curves for different tendon sags (200, 300, and 400 mm) when the tendon cross-sectional area was 48 mm^2 and initial tendon force was 20 kN. As can be seen in this figure, a large tendon sag can ensure more effective reinforcement.

3.3.3. Effects of different parameters on the load-deflection curve

Initial tendon force, tendon cross-sectional area, and tendon sag have different effects on the load-deflection curve for the RC beam:

1. Effect of initial tendon force. **Figure 6a** shows the load-deflection curves for four different initial tendon forces when the tendon cross-sectional area was 48 mm^2 and tendon sag was 200 mm. An analysis of the curves reveals that an increase in the initial tendon force can increase the RC beam's ultimate bearing capacity and reduce the duration of the hardening stage. Decreasing initial tendon force has the opposite effects. As shortened duration of hardening is not expected for structural performance, a greater initial tendon force does

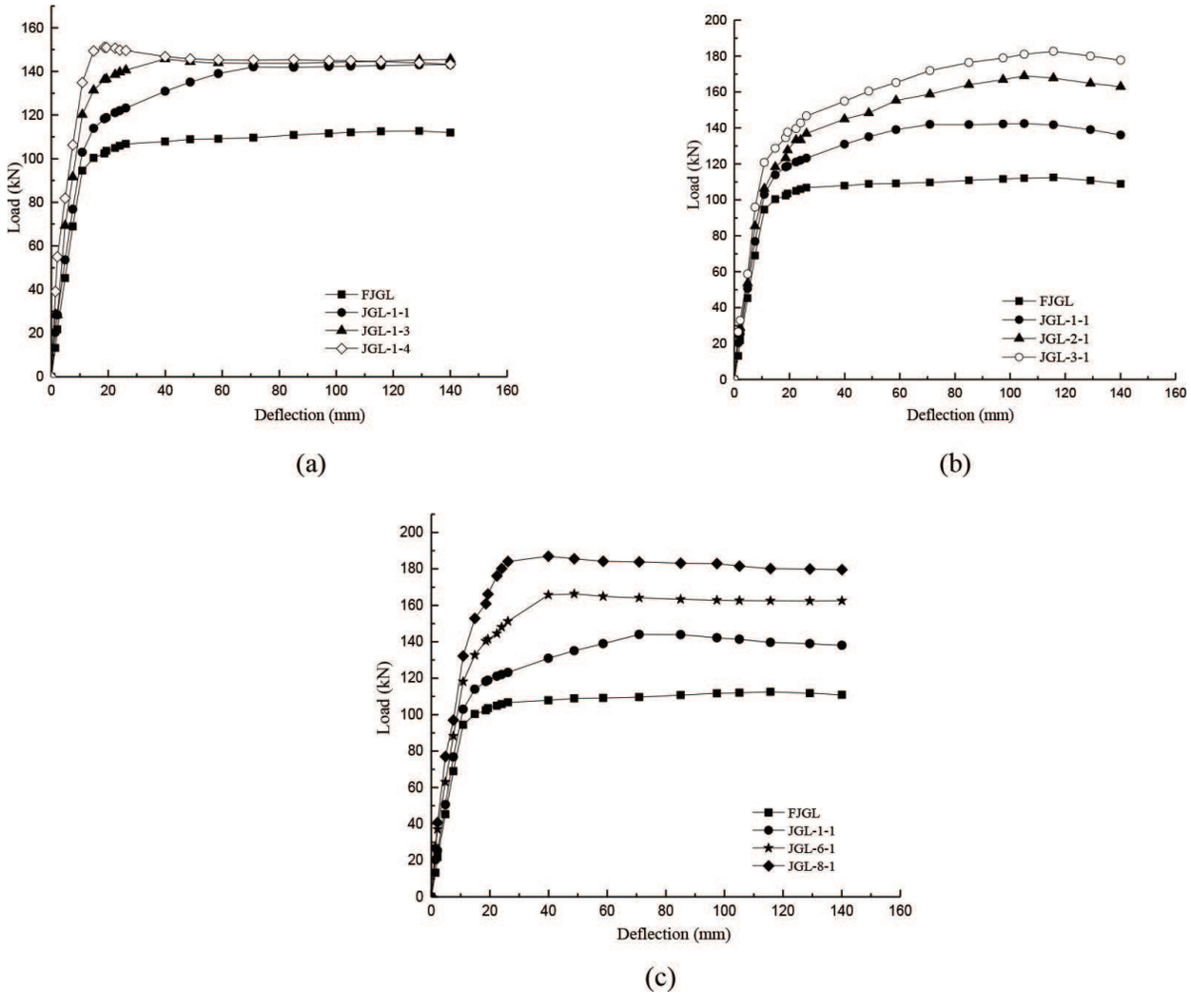

Figure 6. Effect of different factors on strengthening beam. (a) Initial internal force of cable, (b) sectional area of cable, and (c) sag of cable.

not necessarily mean more effective reinforcement. After the initial tendon force exceeded a threshold (53% in this study), the external tendon will yield and fracture in advance and the RC beam becomes more likely to fail by brittle fracture.

2. Effect of tendon cross-sectional area. When the initial tendon force and tendon sag stay unchanged, there is a positive relationship between tendon cross-sectional area and the structural performance of a balanced-reinforced beam. As the tendon cross-sectional area increased, the structure improved both in yield strength and ultimate strength, and the duration of the hardening stage was extended. **Figure 6b** shows the load-deflection curves for different tendon cross-sectional areas and constant initial tendon force (20 kN) and tendon sag (200 mm). When the tendon cross-sectional area was 48, 86, and 134 mm^2, the RC beam's yield strength increased by 15, 22, and 30%, respectively, compared with that of the unreinforced beam. The corresponding increases in the beam's ultimate strength were 16, 37, and 48%. These results demonstrate significant improvement in structural ductility. According to the concept of an over-reinforced beam, there should be an upper limit on tendon cross-sectional area. This needs to be discussed in future research.

3. Effect of tendon sag. When the initial tendon force and cross-sectional area remain constant, the structural performance of the RC beam tends to vary positively with tendon sag. As the tendon sag increased, the structure showed increases in both yield strength and ultimate strength. **Figure 6c** illustrates the load-deflection curves for a tendon specimen with initial tendon force of 20 kN and cross-sectional area of 48 mm^2. When the tendon sag was 200, 300, and 400 mm, the beam's yield strength increased 15, 29, and 45%, respectively, after the reinforcement. The corresponding increases in its ultimate strength were 16, 33, and 48%, respectively. These results suggest great effect of sag on the beam's bearing capacity. When the tendon sag exceeded a threshold (300 mm in this case, equal to beam height), the duration of hardening experienced by the beam was shortened. Further research is needed to verify if this threshold equals beam height in all cases.

3.3.4. Characteristics of plastic zone development

The analysis above shows that the application of DWM external prestressing not only improved the bearing capacity of the SSB but also altered the plastic zone developed in the beam. **Figure 7** shows the contours of stress in the plastic zone throughout the deformation processes of the unreinforced beam and the RC beam. When the unreinforced beam was subjected to an external load, a plastic zone arose first in the beam segment in the stage of pure bending. As the load increased, the plastic zone tended to expand toward the two ends symmetrically about the midspan position. The height of the plastic zone at midspan gradually increased and always peaked around the midspan. The plastic zone within the segment in shear bending gradually expanded from the loading point to the supports.

In the RC beam, the plastic zone in the region corresponding to the pure-bending segment of the unreinforced beam expanded at a slower rate due to the presence of web members. The plastic zone's height decreased compared to that in the unreinforced beam. Along the beam bottom, it was symmetrically distributed about the midspan web member. As the load

http://dx.doi.org/10.5772/intechopen.76517

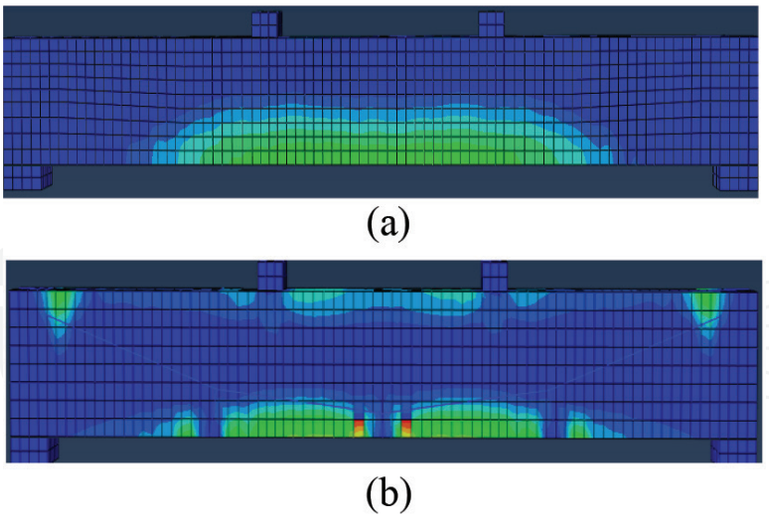

Figure 7. The plastic strain distribution of beam. (a) FJGL and (b) FGL-3-3.

increased, the plastic zone slowly extended toward the top and ends and reached the highest point between web members. The plastic zone area was significantly smaller than that observed in the unreinforced beam. A plastic zone developed at the RC beam top, which is characteristic of deformation of continuous beams. This suggests that after reinforcement, the stress in the beam was redistributed and the properties of the material were used to a greater extent.

4. Tests and results

4.1. Experimental design

Table 1 shows the number of test specimens and their materials. Two parts were prepared for each of the specimens indicated by *. The specimens were divided into three groups. Then "1-" and "2-" were added to the original specimen numbers.

Figure 8 shows the design of the specimens (reinforcement ratio 1.27%). The properties of the rebars, steel wire ropes, and other materials used in the RC beam are presented in **Table 3**. The concrete strength, at 28 MPa, was measured using rebound hammer.

Loading scheme: A three-point bend test was performed on the specimens using a hydraulic servo jack (**Figures 9** and **10**). Each test process was first controlled by load, which increased 10 kN for each stage. After the load reached 100 kN, displacement control was applied, and the displacement increased 5 mm each stage. The loading time was 3 min and the period of sustained load was 30 min.

Observation scheme: (1) observed variables: load, midspan displacement, beam-end displacement, and stress in concrete, wire ropes, rebars, and web members; (2) observation method: measurements by load transducer, displacement meter, and resistance strain gauge and manual measurement record using coordinate paper (rope length change was measured as strain in rope) and calculation using the Hooke's law; and (3) test devices: static strain gauge, ruler, and so on [12].

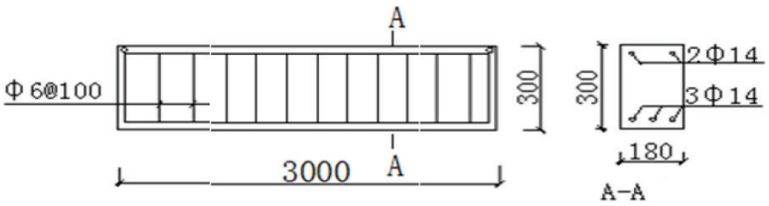

Figure 8. Sectional properties of tested beam (the unit used in the figure is mm).

Name	Diameter Φ (mm)	Density ρ (kg/m³)	E_s (N/mm²) × 10⁵	Breaking force(kN)	Tensile strength (N/mm²)
Wire rope	9	/	1.4	75	1550
Wire rope	15	/	1.4	208	1550
Reinforcement	14	7800	1.95	/	400

Table 3. Material properties table.

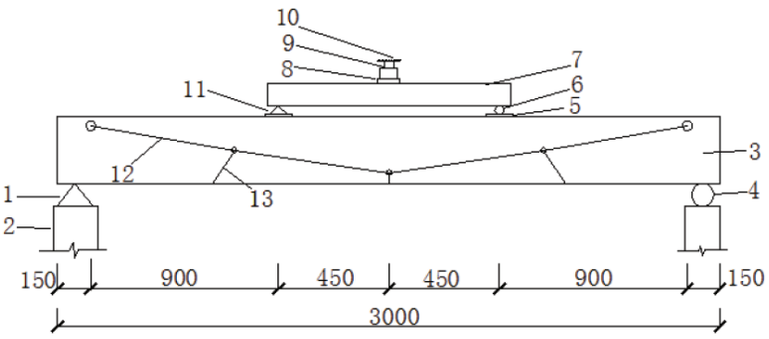

Figure 9. Schematic diagram for loading setup (the unit used in the figure is mm). Notes: (1) fixed hinged support; (2) buttress; (3) test beams; (4) rolling hinged support; (5) backing plate; (6) rolling hinged support; (7) distributive girder; (8) jack; (9) pressure sensor; (10) reaction beam; (11) rolling hinged support; (12) wire rope; and (13) web member.

Figure 10. Load diagram of testing beam.

First, the SSB's mechanical properties before reinforcement were measured, and the results were plotted as load-deflection curves. Stop loading when the maximum fracture width in the concrete in the tensioned region reached 0.2 mm and then unload the specimen. Later, the initial prestressing force was applied to each specimen based on the reinforcement design requirements until the specimen failed.

4.2. Experimental results

4.2.1. Load-deflection curve

Figure 11 compares the load-deflection curves for four specimens before and after reinforcement. When the beam deflection reached 4 mm, specimens 1JGL-1-1, 2JGL-1-1, 1JGL-5-2, and 2JGL-5-2, respectively, showed 29, 30, 41, and 43% increases in load compared to those before reinforcement. For a deflection of 7 mm, the load increased 26, 28, 35, and 37%, respectively, compared with those before reinforcement. The experimental results demonstrate that the specimens became stiffer after the reinforcement.

Figure 12 compares the load-deflection curves for six specimens before and after reinforcement. The fracture strength of specimens 1JGL-1-1, 2JGL-1-1, 1JGL-5-2, and 2JGL-5-2 increased by 21, 26, 38, and 42%, compared to the fracture strength of specimen 2JGL-5-2. Their ultimate strengths were up 13%, 15%, 41%, and 43%, respectively, compared with specimen 2JGL-5-2.

The experimental results show that the reinforcement improved the stiffness of the specimens and resulted in 24 and 40% increases in their fracture strength, 24 and 37% increases in yield strength, and 15 and 42% increases in ultimate strength on average. Specimens with larger tendon cross-sectional areas and sags exhibited better structural performance, consistent with the numerical results.

4.2.2. Failure characteristics

The failure characteristics of the six specimens are presented in **Table 4**. The unreinforced beams were balanced-reinforced. As they failed when the rebars began yielding, their failure mode was ductile failure. The RC beams were divided into two groups: one group with small tendon cross-sectional areas and small tendon sag, and the group with larger tendon cross-sectional areas and larger tendon sags. The rebars all yielded as the tendons failed. The structure ductility was relatively high in both groups. The former group failed before the external tendons fractured, while the latter group failed before the concrete was crushed. This difference demonstrates that large cross-sectional areas and tendon sags in reinforcement design can deliver better results.

4.2.3. Fracture distribution

1-FJGL is an unreinforced beam. When the external load applied to it reached 40 kN, the first fracture arose at midspan. Later, new fractures developed in the pure-bending beam segment at intervals of about 130 mm. A diagonal fracture developed in the shear-bending segment when the external load was 60 kN and continuously propagated upward as the load increased. After the external load exceeded 100 kN, a number of vertical fractures occurred at midspan, resulting in a sharp increase in beam deformation. The load-deflection curve had

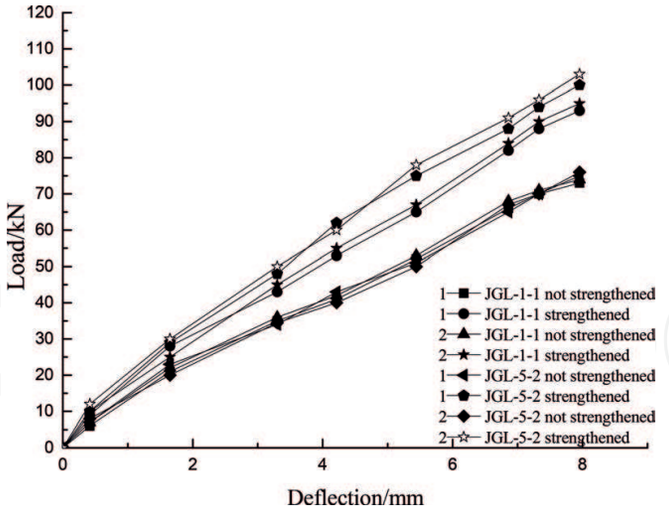

Figure 11. Comparison of bearing capacity between, before, and after reinforcement.

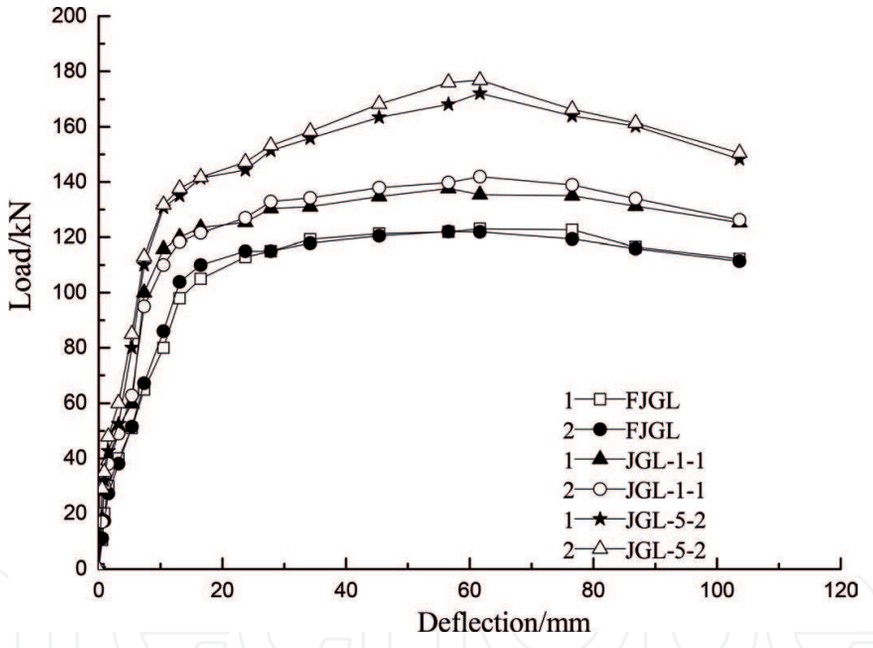

Figure 12. Comparison of load-deflection curves between reinforced beam and unreinforced beam.

only one peak, which corresponded to midspan point in the fractured region on the sides of the specimen (**Figure 13**).

Specimens 2JGL-1-1 and 2JGL-5-2 were loaded until the maximum fracture width reached 0.2 mm. Then they were unloaded and reinforced by a prestressing force. At this point, all fractures in them were closed and the beams formed inverted arches with vertical displacements of 1 mm and 2 mm, respectively.

Beam number	Cable diameter (mm)	Sag of cable (mm)	Internal force of cable (kN)	Cracking load (kN)	Ultimate load (kN)	Failure characteristics
1FJGL	—	/	/	42	124	Ductility
2FJGL	/	/	/	40	115	Ductility
1JGL-1-1	9	200	20	50	136	Broken of cable
2JGL-1-1	9	200	20	53	141	Broken of cable
1JGL-5-2	15	250	30	58	175	Crush
2JGL-5-2	15	250	30	60	180	Crush

Table 4. Characteristic load and failure of beam.

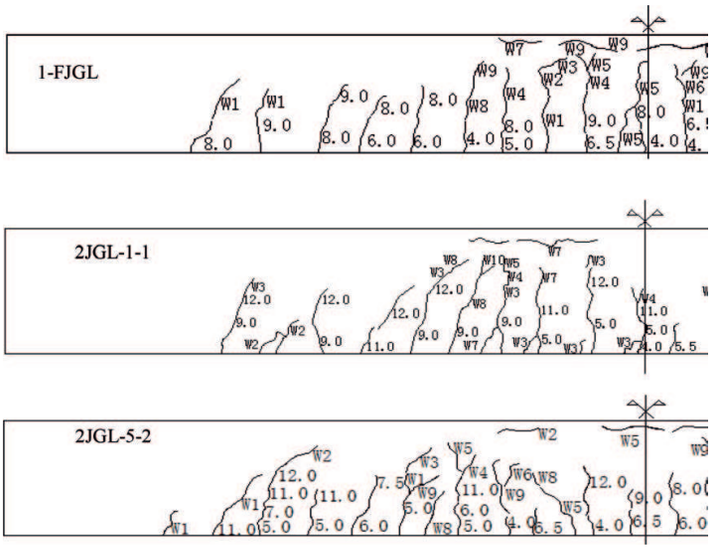

Figure 13. Beam crack mapping. 1-FJGL, 2JGL-1-1, 2JGL-5-2.

Beam number	Yield step		Ultimate load 90%		Displacement ductility ratio (mm)
	Load values (kN)	Displacement (mm)	Load values (kN)	Displacement (mm)	
1FJGL	94	13.5	113	93.9	6.9
2FJGL	99	13.2	116	96.2	7.1
1JGL-1-1	117	14.8	125	146.4	9.9
2JGL-1-1	122	14.1	128	136.2	9.6
1JGL-5-2	133	11.3	152	100.2	8.9
2JGL-5-2	132	10.6	162	85.9	8.1

Table 5. Ductility coefficient of beam.

Specimen 2JGL-5-2. These fracture characteristics of 2JGL-5-2 were similar to those of the previous specimen. Their fracture characteristics differed in two ways: (1) the magnitudes of load at characteristic points were higher than those observed for 2JGL-1-1. For example, the primary fractures opened again when the load was 60 kN and new fractures arose extensively in the shear-bending segment as the load was reached and (2) the four peaks were more obvious in the load-deflection curve for 2JGL-5-2 (See 2JGL-5-2 in **Figure 12**).

The phenomena described above are consistent with the stress contour plots (**Figure 7**), demonstrating the reliability of the analytic method.

4.2.4. Ductility of RC beam

Ductility is an important indicator considered in seismic design for beams. It is usually measured by displacement-based ductility coefficient, μ, [13]:

$$\mu = \Delta u / \Delta y \tag{14}$$

where $\triangle y$ is the displacement when the longitudinal rebars in the beam begin yielding and $\triangle u$ is the displacement when the load is decreased to 90% of the maximum load. The ductility coefficients of the test beams are presented in **Table 5**.

Table 5 reveals that the RC beams had much higher ductility than the unreinforced beams. The specimens with small tendon cross-sectional areas and small initial tendon forces exhibited slightly higher ductility than the specimens with larger tendon cross-sectional areas and greater initial tendon forces.

4.3. Summary

The analysis performed earlier suggests that after being reinforced by DWM external prestressing, the SSB exhibited slightly increased stiffness, improved fracture strength, yield strength, and ultimate strength and significantly increased ductility. This is because the mechanical behavior of the RC beam was constrained by the external prestressing force.

1. It took longer times for the primary microfractures in the concrete to become throughgoing fractures.
2. The beam formed an inverted arch. When an external load was applied, a part of the load would serve to offset the arch displacement.
3. At a point during the experiment, reinforcement system composed of the external prestressing tendons, web members, and beam-bottom anchorage created a “net bag,” which enclosed the working segment of the SSB and caused redistribution of stress at cross-section.
4. Throughout the experiment, the web members served as an elastic support for the beam bottom and resulted in redistribution of internal force in the SSB. The support force provided by the elastic support tended to increase with increasing external load.

http://dx.doi.org/10.5772/intechopen.76517

5. Comparison of the theoretical, numerical, and experimental results

Figure 14 compares the theoretical, numerical, and experimental load-deflection curves for specimens JGL-1-1 and JGL-5-2.

Due to the fundamental assumptions mentioned earlier, the theoretical values for the stage of elastic deformation were slightly smaller than corresponding experimental and numerical values, thus ensuring the safety of the specimens. This demonstrates that the theoretical results can accurately describe the mechanical behavior of the specimens and the calculation method is reliable. For the stage of plastic deformation, the theoretical values were significantly greater than the experimental and numerical values, indicating that the theoretical calculation cannot provide reliable guidance.

The experimental data were highly consistent with the numerical data for both elastic deformation and plastic deformation stages, demonstrating the validity of the numerical method proposed.

Figure 15 compares the structural performance extracted from all experimental curves with the structural performance of the beam models observed in numerical analysis. The findings are as follows:

1. The specimens reinforced by prestressing had better structural performance than unreinforced beams.
2. The structural performance curves fit the numerical and experimental data and roughly move in the same manner, thus confirming the numerical results.

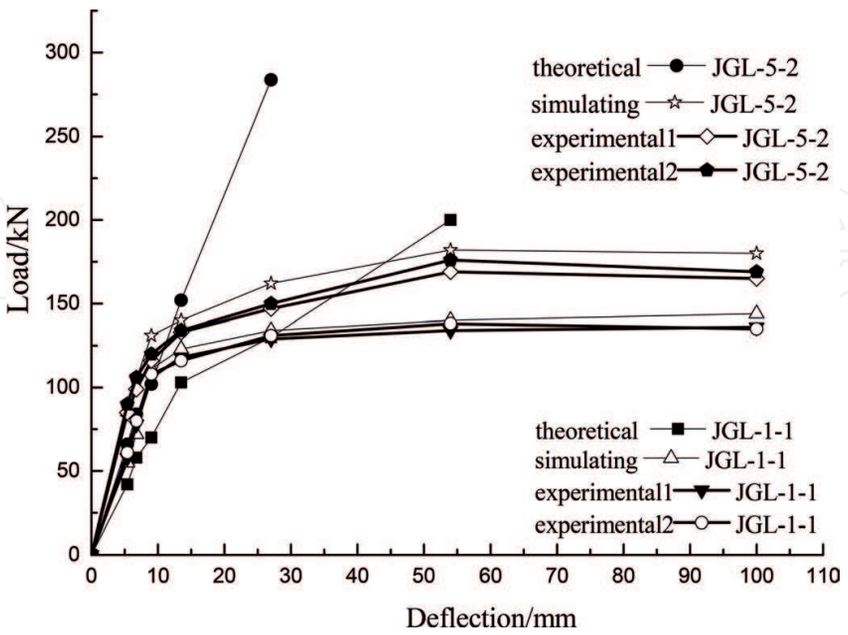

Figure 14. Comparison of theoretical, simulated, and experimental values.

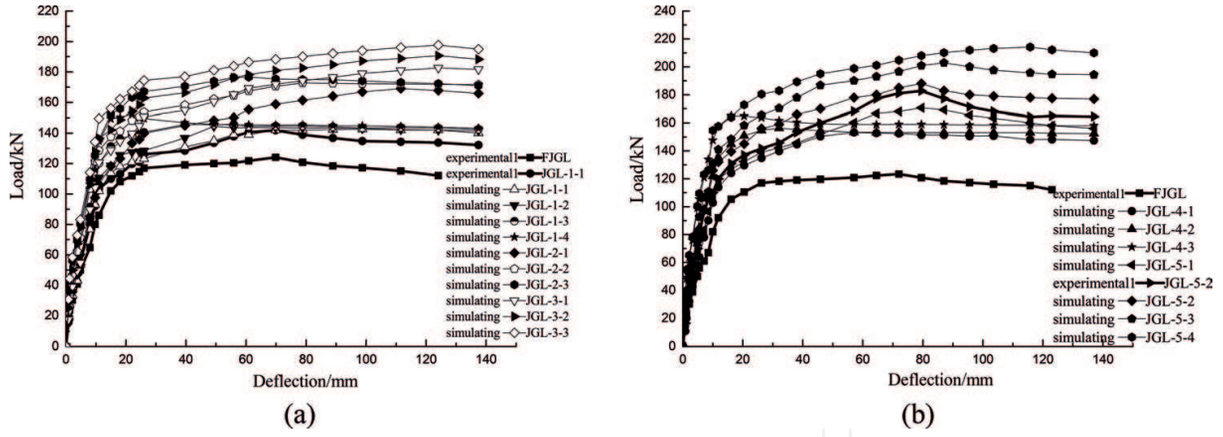

Figure 15. Comparison of simulation value and test value of related specimens. (a) Dip 200 All values contrast and (b) dip 250 All values contrast.

6. Conclusions

1. The load-deflection curve for a RC SSB can be divided into four portions, which correspond to the four deformation stages: elastic deformation, yielding, hardening, and failure. The RC beam specimens failed in two modes: brittle failure of external tendons and ductile failure of concrete in compression.
2. The application of DWM external prestressing results in redistribution of stress at the cross-section of the RC beam, which allows the materials to make greater contribution and improves the beam's structural performance.
3. The theoretical calculation method proposed can deliver reliable results for the stage of elastic deformation and provide a basis for applications in practice.
4. Small tendon cross-sectional areas and high initial stress are not recommended for reinforcement design.

Author details

Teng Wang[1,2]*, Yanmei Ding[1,2], Wangchun Zhang[1,2] and Yu Song[1,2,3]

*Address all correspondence to: wangteng2035@163.com

1 Key Laboratory of Protected Horticulture, Shandong provincial Education Department, Weifang, China

2 Architectural and Civil Engineering Institute, Weifang University of Science and Technology, Weifang, China

3 Western Engineering Research Center of Disaster Mitigation in Civil Engineering of Ministry of Education, Lanzhou University of Technology, Lanzhou, China

References

[1] Yu S. Engineering Structural Detection and Reinforcement. Beijing: Science Press; 2005. pp. 12-15. (in Chinese)

[2] Ting ZY, Jisheng Q, Hengwei H. Survey on research of external pre-stressed concrete beams. Journal of Huazhong University of Science and Technology (Urban Science Edition). 2002;**19**(4):86-91. (in Chinese)

[3] Lou TJ, Lopes AV, Lopes SMR. Influence of span-depth ratio on behavior of externally pre-stressed concrete beams. ACI Structural Journal. 2012;**109**(5):687-695

[4] Ahmed G, Beeby AW. Factors affecting the external pre-stressing stress in externally strengthened pre-stressed concrete beams. Cement and Concrete Composites. 2005;**27**(9-10):945-957

[5] Jinsheng D, Guangda Q. Ultimate stress in external tendons-comments on the existing typical methods. Engineering Mechanics. 2010;**27**(9):63-68 (in Chinese)

[6] He Z, Zhao L, Wang J. A unified algorithm for calculating stress increment of external tendons based on deflection. China Civil Engineering Journal. 2008;**41**(9):90-96. (in Chinese)

[7] Ghallab A, Beeby AW. Calculating stress of external pre-stressing tendons. Structures and Buildings. 2004;**157**(4):263-278

[8] Wu G, Wu Z, Yang W, Jianbiao J, Yi C. Experimental study on flexural strengthening of RC beams with pre-stressed high strength steel wire ropes. China Civil Engineering Journal. 2007;**40**(12):28-37 (in Chinese)

[9] Yu S, Wang Y, Aipeng LI. Internal force analysis of external pre-stressed cable of tilted belly poles. Engineering Mechanics. 2011;**28**(5):143-148. (in Chinese)

[10] Zhu H, Yang Y, Fan W. External Prestressing Bridge Reinforcement Technology Review. International Conference on Engineering Technology and Application (ICETA 2015)

[11] Astawa MD, Raka IGP, Tavio. Moment Contribution Capacity of Tendon Prestressed Partial on Concrete Beam-column Joint Interior According to Provisions ACI 318-2008 Chapter 21.5.2.5 (c) Due to Cyclic Lateral Loads. The 3rd Bali International Seminar on Science & Technology (BISSTECH 2015)

[12] Xu L, Xu F, Hao Z, Wenke Q. The design and test study on pre-stressed railway concert beam -bridge strengthened by externally draped CFRP tendon. Engineering Mechanics. 2013;**30**(2):89-95. (in Chinese)

[13] Vasudevan G, Kothandaraman S. Experimental investigation on the performance of RC beams strengthened with external bas at soffit. Materials and Structures. 2014;**47**(10):1617-1631

IntechOpen